You might find this additional information useful...

This article cites 17 articles, 1 of which you can access free at:
http://jn.physiology.org/cgi/content/full/98/6/3759#BIBL

Updated information and services including high-resolution figures, can be found at:
http://jn.physiology.org/cgi/content/full/98/6/3759

Additional material and information about *Journal of Neurophysiology* can be found at:
http://www.the-aps.org/publications/jn

This information is current as of January 7, 2008 .

Applying Double Magnetic Induction to Measure Two-Dimensional Head-Unrestrained Gaze Shifts in Human Subjects

Peter Bremen, Robert F. Van der Willigen, and A. John Van Opstal
Department of Biophysics, Institute for Neuroscience, Radboud University Nijmegen, Nijmegen, The Netherlands

Bremen P, Van der Willigen RF, Van Opstal AJ. Applying double
magnetic induction to measure two-dimensional head-unrestrained
gaze shifts in human subjects. *J Neurophysiol* 98: 3759–3769, 2007.
First published September 26, 2007; doi:10.1152/jn.00886.2007. This
study compares the performance of a newly developed gaze (eye-in-
space) measurement technique based on double magnetic induction
(DMI) by a custom-made gold-plated copper ring on the eye with the
classical scleral search coil (SSC) technique to record two-dimen-
sional (2D) head-unrestrained gaze shifts. We tested both systems
simultaneously during head-free saccades toward light-emitting
diodes (LEDs) within the entire oculomotor range (± 35 deg). The
absence of irritating lead wires in the case of the DMI method leads
to a higher guarantee of success (no coil breakage) and to less
irritation on the subject's eye, which results in a longer and more
comfortable measurement time. Correlations between DMI and SSC
signals for horizontal and vertical eye position, velocity, and acceler-
ation were close to 1.0. The difference between the SSC signal and the
DMI signal remains within a few degrees. In our current setup the
resolution was about 0.3 deg for the DMI method versus 0.2 deg for
the SSC technique. The DMI method is an especially good alternative
in the case of patient and laboratory animal gaze control studies where
breakage of the SSC lead wires is particularly cumbersome.

INTRODUCTION

At present, two invasive electromagnetic methods for mon-
itoring eye movements are being used in oculomotor research:
the scleral search coil (SSC) technique (Collewijn et al. 1975;
Robinson 1963) and the double magnetic induction (DMI)
method (Allik et al. 1981; Bos et al. 1988; Bour et al. 1984;
Malpelli 1998; Reulen and Bakker 1982). Temporal and spatial
resolutions of both methods are comparable when recording
head-restrained eye movements. However, whereas the SSC
technique can be readily used to measure head-unrestrained
two-dimensional (2D) gaze shifts, the DMI method so far has
been restricted to head-fixed experimental settings only. Two
problems inherent to the DMI method make its use somewhat
tedious. To understand these it is necessary to briefly review
the theoretical and practical background of DMI.

The DMI method makes use of a gold-plated short-circuited
copper ring that is placed on the subject's eye instead of a
silicon annulus with an embedded copper coil, as is the case for
the SSC technique. Because the ring is not connected to the
recording apparatus, a coil that picks up the tiny secondary
magnetic field generated by the primary currents in the ring
(thus double magnetic induction) has to be placed in front of
the eye.

Note that the pickup coil also records the much stronger
signal of the primary magnetic fields generated by the field
coils, which are not related to the eye-in-head orientation. An
anticoil that is connected antiparallel to the pickup coil should
therefore cancel these components. In practice, however, it is
not possible to perfectly cancel the primary field contributions,
resulting in DC components that depend in a complicated way
on the head orientation and on small electromagnetic differ-
ences between pickup coil and anticoil. This DC together with
the eye signal's nonmonotonic nonlinearity have been consid-
ered a serious problem for the application of DMI to head-
unrestrained situations.

In a recent paper (Bremen et al. 2007) we described the
theoretical background needed to extend the classical DMI
method to head-unrestrained conditions. For example, the
signal induced by the horizontal magnetic field, as recorded by
the pickup coil, is described by the following equation

$$V_h(\alpha, \gamma, t) = K(t) \sin (\alpha + \gamma) L(\cos \alpha) + V_{net}(\gamma, t) \qquad (1)$$

where V_h is the voltage recorded by the pickup coil, α is the
horizontal eye-orientation in the head, γ is the horizontal
head-orientation in space, and t is time. $K(t)$ is a coefficient that
includes the characteristics of the time-varying primary mag-
netic field, the ring geometry, and the electromagnetic proper-
ties of the pickup coil. $L[\cos (\alpha)]$ is a nonmonotonic geomet-
rical shape factor that is determined only by the ring/pickup
coil geometry. This shape factor distinguishes the DMI method
from the SSC technique, for which $L[\cos (\alpha)] = 1$ (Bos et al.
1988). V_{net} describes the head-orientation–dependent DC that
is due to imperfect cancellation of the primary field component
(Bremen et al. 2007). Note that the shape factor depends only
on eye-in-head orientation, whereas V_{net} depends solely on
head orientation in space.

As a consequence of the complicated three-dimensional
(3D) geometrical relationship between ring and pickup coil, the
effective measurement range is limited to about 30 deg because
the nonlinear relation between gaze orientation and signal
strength is nonmonotonic. The linear range, being about ± 10
deg, is even more restricted (Bos et al. 1988; Reulen and Bakker
1982). Additionally, the exact ring–pickup coil geometry
strongly influences the measurement range and the signal/ring-
orientation relation. If the ring is positioned slightly off-center
relative to the pickup coil the shape factor also changes,
thereby shifting the nonmonotonic part of the signal. This
creates a pronounced signal asymmetry, which may further
reduce the effective measurement range (Bremen et al. 2007).

For these reasons the SSC technique is still widely used and is considered the gold standard. However, especially in experimental animals and patients, the vulnerable lead wires needed to connect the SSC to the recording hardware have proven to pose a considerable risk because they are prone to breakage. Because the DMI method uses a gold-plated copper ring without connecting wires this risk is absent. Therefore should it be possible to extend the DMI method to head-unrestrained conditions, it could serve as a valuable alternative to the widely used SSC technique.

To use DMI in head-unrestrained subjects, the measurement range should not be restricted by the nonmonotonic, and thus ambiguous, dependence of the signal on gaze angle $\alpha + \gamma$ (*Eq. 1*). In our previous paper we demonstrated that introducing an additional, frontal, magnetic field might suffice to resolve the signal ambiguity. In addition, a model-free artificial neuronal network could solve the relatively complex, and in principle unknown, signal asymmetries that are introduced by imperfections in the ring–pickup coil geometry and the magnetic fields and can account for the head-orientation–dependent offsets (Bremen et al. 2007).

Yet, the system has so far not been tested on real subjects performing in 2D gaze-orienting tasks. A serious problem of DMI is the strong dependence of the shape factor $L[\cos(\alpha)]$ on the ring–pickup coil geometry. Any shift of either of the two coils relative to the induction ring will strongly influence the signal. In addition, mechanical vibrations of the coils relative to the head (and thus the ring) will introduce unwanted low-frequency noise to the signals, which strongly affect the system's resolution and signal-to-noise (S/N) ratio. Preventing these problems necessitates a rigid and vibration-free pickup coil/anticoil assembly, which so far has been achieved only in head-restrained subjects (Bour et al. 1984; Malpeli 1998). The present study demonstrates that all these potential problems can be overcome with relatively simple means. We show experimental data obtained with a low-cost custom-made pickup coil/anticoil assembly applied to human subjects who made rapid 2D head-unrestrained gaze shifts. We also present a simple routine to calibrate the system. We tested our method over a range of ± 35 deg in all directions and compared the calibrated signals to simultaneous recordings obtained from the classical SSC technique that was applied to the other eye. Our results show that, despite a slightly lower resolution (0.3 vs. 0.2 deg), the extended DMI method is a good and low-cost alternative to the search-coil technique for measuring 2D gaze shifts, in principle over the entire motor range.

METHODS

Subjects

Three male subjects participated in these experiments (JG, PB, and RW). Ages ranged from 27 to 40 yr. In all three subjects simultaneous recordings with the SSC technique and DMI method were performed. To familiarize the subjects with the paradigms, a short practice session was performed before the first experimental session. Subjects PB and RW are authors of this paper. Subjects JG, PB, and RW had corrected-to-normal vision (JG: -3.5D right, -3.5D left; PB: -3.5D right, -3.0D left; RW: -2.8D right, -2.0D left) but did not wear their glasses during the experiments. All subjects were experienced in oculomotor studies and participated on a voluntary basis. Experiments were performed in accordance with the Declaration of Helsinki.

Apparatus

Experiments were conducted in a completely dark room ($3 \times 3 \times 3$ m³). Three orthogonal pairs of single-turn field coils (surface area 6 mm²) used to generate the primary magnetic field were mounted alongside the edges of the four walls, ceiling, and floor. The coils were driven by a Remmel field-generating system (Remmel 1984; EM 7 Remmel Labs, Katy, TX; horizontal field: 48 kHz, vertical field: 60 kHz, frontal field: 80 kHz). To monitor eye movements and to have a direct comparison of the DMI method with the SSC technique, the subjects wore a gold-plated copper ring (custom made, thickness 0.3 mm, inner diameter 11.3 mm, top angle 108 deg, weight 0.46 g; also see Fig. 4 in Bour et al. 1984) on the right eye, and the SSC (Scalar Instruments, Delft, The Netherlands) on their left eye. Before insertion of the ring and the coil both eyes were anesthetized with two drops of oxybuprocain [0.4%, in HCl (pH 4.0), Thea Pharma S.A., Wetteren, Belgium]. Both ring and coil were manually inserted without the aid of a suction device. To that end, the subject was requested to look downward while the upper eyelid was lifted, so that the ring/coil could be gently inserted. Subsequently, the ring/coil was positioned in the frontal plane around the cornea, with the aid of a wetted cotton swab, if needed (Fig. 1, *A* and *C*). The coil's lead wires were secured with tape to the nose and forehead. After the experiments the ring/coil apparatus was removed with a blunt forceps.

The ring's secondary magnetic field was registered with a pickup coil placed in front of the eye. The pickup coil and the anticoil (both: surface area of the wire 0.13 mm², 35 turns, ∅ of the coil 2.5 cm, L = 120 μH, DC resistance 1.8 Ω, connected in series) were mounted on a lightweight plastic glasses frame (total weight: 148 g; hereafter referred to as the DMI assembly) that was worn by the subjects (Fig. 1, *A–C*). To reduce noise that appeared to be caused by skin contact, the coils were further insulated with a thin layer of silicon. The DMI assembly was constructed such that both coils remained in the same plane and thus had the same orientation relative to the primary magnetic fields. A rubber strap around the subject's head connected the temples of the glasses frame to further tighten the assembly. The DMI assembly was sufficiently rigid so that it did not slip or distort when the subject made rapid head-unrestrained gaze shifts. The distance between pickup coil and eye varied from subject to subject but ranged between 1.5 and 2.0 cm. In some subjects play dough (Play-Doh, Hasbro) was molded around the nose bridge to roughly center the pickup coil in front of the ring, to optimize the field of view (± 30–35 deg in both directions) and to achieve a comfortable fit of the glasses frame.

Horizontal and vertical head movements were measured with the search-coil technique. For that purpose a small custom-made coil was wound around a miniature laser device (LQB-1-650, World Star Tech, Toronto, Ontario, Canada; see *Stimuli*) that was mounted on the nose bridge of the glasses frame (Fig. 1, *A* and *C*).

The head coil (horizontal and vertical channels) and gaze signals (DMI and SSC: horizontal, vertical, and frontal channels) were amplified (total of eight channels), demodulated, and low-pass filtered at 150 Hz (fourth-order Butterworth, custom built) before being stored on hard disk at a sampling rate of 500 Hz/channel for subsequent off-line analysis.

Stimuli

Subjects were seated comfortably in the center of the experimental chamber facing a spherical wooden frame (radius: 85 cm) with 12 spokes and five concentric rings (LED sky; described in detail in other studies from our lab, e.g., Hofman and Van Opstal 1998). A polar coordinate system with its origin at the straight-ahead position was defined to describe target positions. Target eccentricity (R) is measured as the angle with respect to the straight-ahead position, whereas target direction (ϕ) is measured relative to the horizontal meridian. LEDs (0.2 deg diameter as viewed by the subject, intensity 0.15
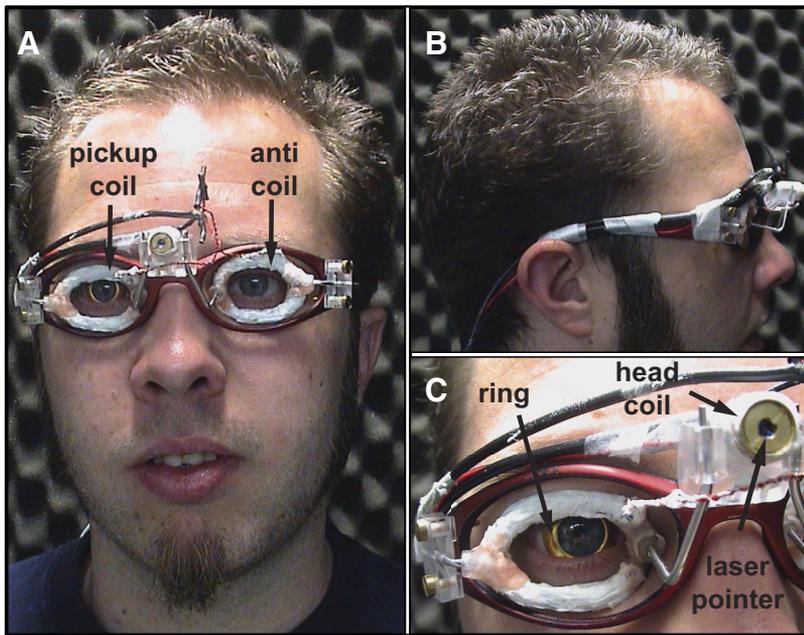
FIG. 1. Subject wearing coil assembly and ring. *A*: frontal view. Note that the coils are elliptical and isolated from the skin with white silicon rubber. Elliptical shape optimized the subject's horizontal field of view and allowed putting the pickup coil closely in front of the ring. Signal strength could thus be optimized. A small laser pointer was mounted on the nose bridge and a coil to measure head orientation is wound around it (not visible). Ring on the subject's right eye is made from thin gold-plated copper and fits around the subject's cornea. Ring is not embedded in silicon, as is the case with the scleral search coil (SSC). *B*: side view. *C*: close-up of the pickup coil, ring, and laser pointer.

cd·m^{-2}) were mounted at R = {0, 2, 5, 9, 14, 20, 27, 35} deg (rings) and ϕ = {0, 30, 60, ... , 330} deg (spokes) on the frame. For example, the position of the center LED is described by (R, ϕ) = (0, 0) deg. A target in the upper right quadrant can be described by (R, ϕ) = (14, 60) deg and one in the lower left quadrant as (R, ϕ) = (9, 240) deg. For off-line analysis these polar coordinates were transformed into their corresponding azimuth (α) and elevation (ε) angles (Hofman and Van Opstal 1998) by

$$\alpha = \arcsin (\sin R \cos \Phi)$$
$$\varepsilon = \arcsin (\sin R \sin \Phi) \qquad (2)$$

respectively.

In addition to these LEDs the small laser device mounted on the nose bridge of the glasses frame was used to align the subject's head to the target (see *Paradigms*).

Paradigms

All experiments were performed in darkness.

CONTROL EXPERIMENT. To ensure that there was no interference of the SSC on the DMI assembly and vice versa two control experiments were performed with subject JG (SSC and DMI assembly without ring; DMI assembly and ring without SSC) that showed that the respective signal was not disturbed (data not shown).

CHARACTERIZATION OF V_{NET}. We conducted measurements with subjects wearing the assembly without ring and SSC to characterize the head-orientation–dependent remnant primary field component (referred to as V_{net} in *Eq. 1*) picked up by the DMI assembly and to assess whether it remains stable during the course of an experimental session. In addition, we recorded the signal from the head coil to have a standard with which to compare the V_{net} signal. The subjects had to align the head-fixed laser pointer to targets presented in pseudorandom order on the LED sky (see following text). Each target location was presented four times to test the stability and reproducibility of the assembly.

EXTENDED DMI METHOD. In the actual recording experiments we conducted measurements while subjects wore the DMI assembly, ring, and SSC. Two paradigms were used: *1*) a closed-loop calibration experiment (Fig. 2, *A* and *B*) and *2*) a test experiment (Fig. 2*C*).

Each trial in the calibration paradigm started with a green fixation LED at (R, ϕ) = (2, 0) deg, which was presented for 800 ms. The subject had to align the head-fixed pointer to that fixation LED. This procedure ensured that the head was at the same starting position for every trial. The fixation LED was then first followed by the so-called head target (red LED) that remained lit until the end of the trial. The subject had to align the head-fixed pointer, and thus his head, to this target LED and keep it there for the remainder of the trial. After 1,500
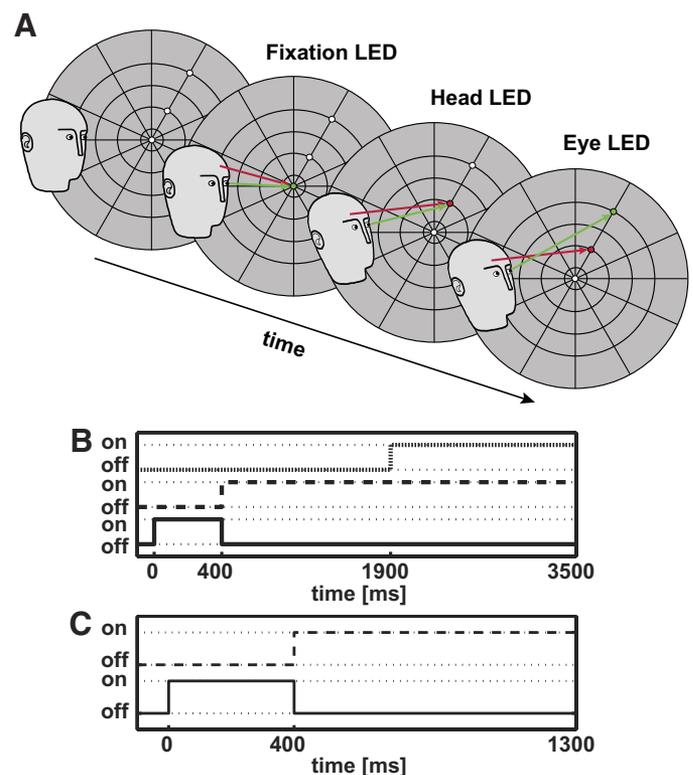
FIG. 2. Paradigms used for calibration and testing. *A*: cartoon of one trial of the calibration paradigm. *B*: time sequence of the calibration paradigm. *C*: time sequence of the test paradigm. F, Fixation light-emitting diode (LED); T, Target LED; T$_H$, Head target LED; T$_E$, Eye target LED.

ms a second target LED (green, the so-called eye target) was lit for 1,600 ms. The subject had to make an eye saccade to this new target *without moving the head.*

A series of computer simulations in one dimension was performed (Bremen et al. 2007) to determine the minimal number of different head–eye combinations needed for a successful calibration. Typically, only five eye positions along the same direction ϕ as the head (two at the extreme opposite ends of the oculomotor range and one at the center) for each given head position sufficed. This ensured that most of the points were sampled at the nonlinear and nonmonotonic part of the ring's eye-in-head signal (see Fig. 7). Each target pair was repeated three times.

In the test paradigm the offset of the central fixation LED was immediately followed by the appearance of a peripheral target that remained lit for 900 ms. The subject was instructed to make a natural orienting gaze shift with both the head and eye toward this target, as quickly and as accurately as possible. To elicit large gaze shifts the head-fixed pointer remained on during the test paradigm. For all experiments, the order of stimulus conditions and positions was randomized throughout a session. One recording session lasted for 30 to 40 min, of which about 10 min were used for calibration. Note that the maximum recording time was restricted by the SSC. The lead wires typically become increasingly irritating during the course of an experiment, eliciting disturbing blinks. Because the ring is less irritating due to the lack of lead wires it can be worn for ≤60 min (Bour et al. 1984).

Calibration

Before off-line calibration, the data were digitally low-pass filtered at 75 Hz using a 50-point FIR (finite impulse response) filter. Fixation endpoints were determined off-line. A window with duration of 100 ms around saccade offset determined the average endpoint values of the eye- and head-position signals. The window was adjusted after visual inspection to correct for errors. Endpoints were averaged (V_{net}: four repeats per target location; DMI/SSC: three repeats per target combination) after removing outliers.

For both the V_{net} and the DMI/SSC measurements, the head coil signal was calibrated using two three-layer feedforward neuronal networks for the horizontal and vertical components of the head movement. The input to the networks consisted of the horizontal and vertical voltages as recorded with the head coil. Input units were connected to four hidden units that projected to the output unit of the networks. The networks were either trained on the whole data set (V_{net}) or on the set of data points collected during the head target epoch of the calibration paradigm (DMI/SSC). The networks' output was the horizontal or vertical head orientations in space, $H\alpha$ and $H\varepsilon$, respectively.

Networks were trained by the Bayesian-Regularization implementation of the back-propagation algorithm (Matlab 7.0, Neural Networks Toolbox, The MathWorks) to avoid overfitting (MacKay 1992).

CHARACTERIZATION OF V_{NET}. Although V_{net} is only a head-orientation–dependent DC we mapped it on the target positions in space. This allowed us to better assess the stability and reproducibility of the DMI assembly and to compare the amplitude of V_{net} with the calibrated head coil signal.

For this, the pickup coil signals were calibrated with two three-layer feedforward neuronal networks for the horizontal and the vertical components, respectively. Three input units—*1)* voltage of the horizontal field V_h, *2)* voltage of the vertical field V_v, *3)* voltage of the frontal field V_f—were connected to four hidden units that projected to one output unit yielding horizontal ($H\alpha$) and vertical ($H\varepsilon$) head orientation, respectively. The networks were trained on a total of 67 averaged endpoints with the teacher value being the target location in space. The thus trained networks were subsequently used to calibrate the raw endpoints for all target repetitions.

EXTENDED DMI METHOD. DMI and SSC signals were both calibrated with three-layer feedforward neuronal networks. Note that for the calibration of the ring signal it is not necessary to subtract the complicated V_{net} contribution. The networks used for calibration automatically take V_{net} into account.

Horizontal and vertical components of saccades were calibrated independently. The four input units of the networks were *1)* voltage of the horizontal field V_h, *2)* vertical voltage of the vertical field V_v, *3)* voltage of the frontal field V_f, and *4)* either $H\alpha$ or $H\varepsilon$ (calibrated with the above-mentioned neuronal networks), whereas the desired, single output of the network was the gaze angle, $G\alpha$ or $G\varepsilon$. The networks, which contained one layer of four hidden units, were trained on a total of 109 head–eye combinations (27 head–eye combinations × 4 axes + mean fixation LED value) collected during the eye target epoch of the calibration paradigm. Networks were trained within 1 min. After training, the networks were used to calibrate the test data.

Data analysis

To assess how well the networks approximated the data, linear fits of target position versus network output were performed. If not stated otherwise all linear fits were made using the least-squares criterion.

CHARACTERIZATION OF V_{NET}. The four calibrated target repeats were used to assess whether the DMI assembly remained stable during the recording session. The mean endpoint for a given target location was calculated and the four corresponding repetitions were subtracted from this mean to obtain an estimate of the variability. These procedures were performed for the DMI assembly and the head coil signal.

EXTENDED DMI METHOD. We performed a spectral analysis of all trials recorded during the test experiment for each subject. For this, we applied a 512-point fast Fourier transform to the horizontal and vertical components of both the DMI method and the SSC technique. Subsequently the spectra were averaged for each subject. This analysis would show, for example, whether the DMI assembly introduces characteristic vibrations to the ring signal.

To provide an estimate of the resolution of the extended DMI method and the SSC technique we calculated the SD over 100 calibrated samples taken from the fixation epoch and all target positions of the test experiment. This was done independently for the horizontal and vertical components and for each subject. Subse-
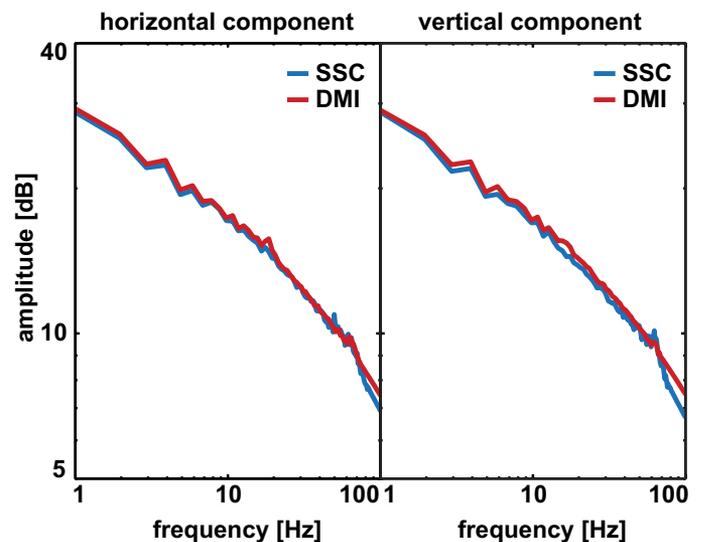
FIG. 3. Average power spectra for the horizontal (*left*) and vertical component of the double magnetic induction (DMI) method (red) and the SSC technique (blue). Spectra for all trials of the test experiment from subject RW were calculated and subsequently averaged.

TABLE 1. *Resolution in degree calculated as the SD over 100 samples taken from the fixation epoch of the test experiment for all subjects*

Method and Component	Subject			Mean all Subjects
	JG	RW	PB	
DMI horizontal	0.12	0.37	0.37	0.29
SSC horizontal	0.10	0.22	0.15	0.16
DMI vertical	0.23	0.29	0.49	0.34
SSC vertical	0.28	0.24	0.17	0.23

quently, the values obtained for each subject were averaged. We argue that the SD provides a measure of the resolution because it is the root-mean-square (RMS) deviation from the arithmetic mean. Thus it provides information about the magnitude of the noise inherent to the system. Because the noise level determines the lower detection limit, a signal must be bigger than this limit to be detected.

Additionally, we calculated the track velocity and track acceleration for all saccades and subjects by applying a two-point difference differentiation algorithm on the radial gaze position data.

R E S U L T S

We performed a power spectrum analysis of the horizontal and vertical gaze-position data of the DMI and SSC signals of each subject (see METHODS) and for all trials. The spectra did not show any peculiarities on the horizontal and vertical signal components for either the DMI method or the SSC technique, or between the horizontal and vertical components of the signals. In Fig. 3 the average spectra across all trials of the test experiment from subject RW are shown. Horizontal and vertical components are depicted in the *left* and *right columns*, respectively. The DMI signal is drawn in red and the SSC signal in blue. All signals are in good agreement. These data ascertain that the DMI assembly did not introduce spurious mechanical vibrations to the ring signal.

Table 1 lists the resolutions obtained in our current setup for the DMI method and the SSC technique for all subjects. The values are in good agreement with the resolution of the DMI method ($\sim$0.3 deg) being slightly inferior to the SSC technique ($\sim$0.2 deg). Similar resolution values were obtained for fixations across the whole tested range. Only extreme gaze fixations (i.e., beyond $R = 30$ deg) tended to yield somewhat lower resolutions (between 0.3 and 0.6 deg) for both the DMI method and the SSC technique. Yet, the DMI resolution is of the same

order as, or better than, the optimal resolution of the oculomotor system, which is limited by the fovea to about 0.6 deg.

In what follows, we will first present the results of the V_{net} characterization before we describe the results of the DMI/SSC measurements.

Characterization of V_{net}

Figure 4 depicts the mean raw endpoints of both the DMI assembly (*left*) and the head coil (*right*) for subject PB. The head coil endpoints clearly mirror the stimulus array, indicating that the coil's signal varies almost linearly with target position for the range tested. The net DMI assembly signal, in contrast, is highly asymmetric. Note that an ideal assembly would yield a V_{net} of zero for all head positions. In practice the pattern is more complicated. Here, the vertical signal is strongly compressed in the lower hemisphere. This is a feature of the current assembly. Different pickup coil/anticoil geometries will produce different V_{net} shapes, and it is apparent that it would be difficult to describe V_{net} analytically. The compensation of the anticoil is far from perfect because the remnant signal's amplitude reaches about 30% of the head coil signal's maximum amplitude. This remnant signal (maximum value of V_{net}), however, is small enough to allow for a sufficiently large ring signal (e.g., Figs. 7 and 8).

The calibration networks were nevertheless able to linearize the data and thus could account for the head-induced DC (Fig. 6) as well as the complex changes in V_{net} (Fig. 4). Table 2 lists the best-fit parameters of the linear regressions performed on network output versus target position for both the pickup coil and the head coil. The coefficient of determination (r^2) exceeded 0.99 for horizontal and vertical components in both cases. Correspondingly, the RMS error values were small. The values obtained for the pickup coil were slightly higher than those for the head coil. This holds especially for the vertical component with its pronounced asymmetry. However, all gains were close to 1 deg and the offsets close to 0 deg, also indicating that the networks were able to fit the data well.

In Fig. 5 the variation around the mean endpoint of the four fixations of a given target is plotted as function of horizontal (*left*) and vertical (*right*) target positions, for both the DMI assembly (red circles) and the head coil (blue diamonds). The DMI- and head-coil distributions overlap considerably. In addition, it is clear that the endpoint variability does not vary in a systematic way with target eccentricity. The SDs are <2
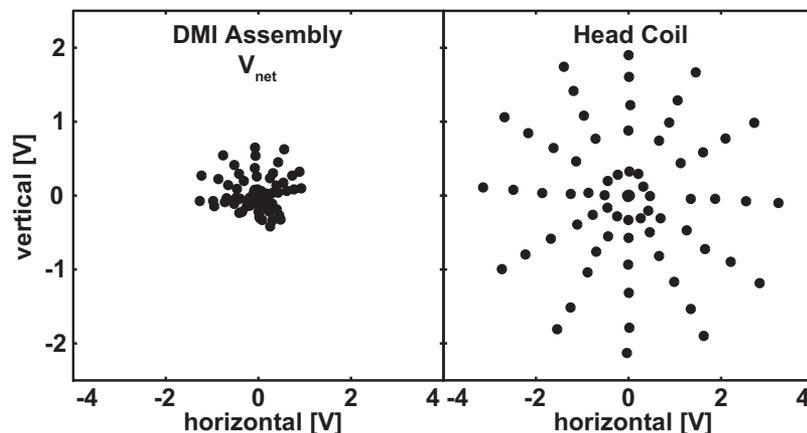
FIG. 4. Uncalibrated endpoints for the DMI assembly (V_{net}) (*left column*) and the head coil (*right column*) for subject PB. Note that an ideal DMI assembly would yield a V_{net} of zero for all head orientations. Here, the vertical endpoints for the DMI assembly are strongly compressed in the lower hemisphere.

TABLE 2. *Coefficients of the fits between the neuronal network output and the teacher value for horizontal and vertical components of the DMI assembly and the head coil for subject PB*

95% Confidence Intervals					
Slope	Intercept	Adj. r^2	RMSE	N	Technique/Component
0.997 (0.987 1.007)	−0.033 (−0.182 0.116)	0.99	0.61	67	DMI assembly horizontal
0.995 (0.977 1.015)	0.027 (−0.258 0.312)	0.99	1.17	67	DMI assembly vertical
1.000 (0.993 1.007)	0.002 (−0.101 0.104)	0.99	0.42	67	Head horizontal
0.997 (0.991 1.004)	−0.027 (−0.130 0.073)	0.99	0.41	67	Head vertical

deg for both methods and components. The distributions for the DMI assembly and the head coil do not significantly differ from each other (Student's *t*-test, $P < 0.01$).

From these data we conclude that the DMI assembly remained stable during a recording session.

DMI/SSC measurement

UNCALIBRATED DATA.   Uncalibrated ring signals for the end-point fixations on the horizontal meridian, as measured during the calibration paradigm, are shown in Fig. 6 (subject PB). These signals were in good agreement with the theoretical predictions described in our previous paper (Bremen et al. 2007). Note that because each line represents one head orientation, a head-orientation–dependent offset can be seen, which is due to two factors: *1*) a head-orientation–related component in the ring signal [the $\sin(\alpha + \gamma)$ term in *Eq. 1*] and *2*) a DC resulting from nonperfect cancellation of the primary field signals (V_{net}). In addition, it is apparent that the combination of horizontal, vertical, and frontal field signals together with the known head orientation uniquely defines the 2D gaze orientation.

Figure 7 depicts the uncalibrated raw endpoints of subject PB recorded during the calibration paradigm. DMI signals are shown in the *left column*, SSC signals are shown in the *center column*, and head-coil signals (used for both methods) are shown in the *right column*. Recall that in the calibration paradigm a head target is followed by an eye target. Endpoints for the former are shown in the *top row* and those for the latter in the *bottom row*. Note that the signals for all three techniques are somewhat asymmetric because the vertical range is smaller than the horizontal range. This is due to the Remmel recording hardware, for which field-driving frequency and signal strength are inversely related; i.e., the lower the frequency, the larger

the signal. The asymmetry between horizontal (field driven at 48 kHz) and vertical (field driven at 60 kHz) components is most prominent for the head-coil signal, for which the vertical amplitude reaches about 65% of the horizontal amplitude. The asymmetry is less pronounced for the DMI signal (74%) and least pronounced for the SSC signal (86%). However, the head-target endpoints for both the DMI method (*left*) and the SSC technique (*center*) are quite similar. Although it is possible to recognize the spatial arrangement of the eye targets by looking at the raw SSC endpoints (*center bottom*), this is less obvious for the DMI endpoints. Here, the more complex geometric dependence of the DMI method (*Eq. 1*) becomes apparent. Nevertheless, as subsequently described, it is possible to calibrate the more complex ring signal, such that the differences between the DMI method and the SSC technique disappear. Note also that the head-coil signal during the head-target epoch (*top right*) and the eye-target epoch (*bottom right*) are virtually identical, indicating that the subject indeed held his head stable during the two epochs.

CALIBRATION.   Figure 8 shows linear regressions that compare the goodness of fit for the network calibrations of the DMI method and the SSC technique for the horizontal and vertical components for subject PB. The corresponding coefficients are listed in Table 3. *Insets* depict the network errors, i.e., teacher value minus network output value. The linear regressions for the two systems were in good agreement, indicating that the networks were well able to fit the DMI data. However, the network errors for the DMI method were slightly larger than those for the SSC technique. SD values (σ) for the DMI method were 0.72 deg for the horizontal and 0.62 deg for the vertical component. For the SSC technique the σ values were 0.30 and 0.32 deg for horizontal and vertical components, respectively.
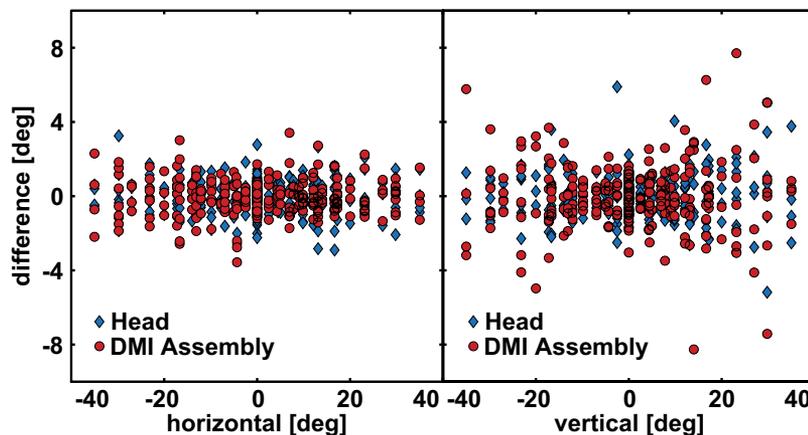
FIG. 5.   Difference of calibrated mean endpoint of a given target and 4 repetitions made to the same target as a function of horizontal (*left*) and vertical (*right*) target position for V_{net} of the DMI assembly (red circles) and the head coil (blue diamonds). Subject PB.
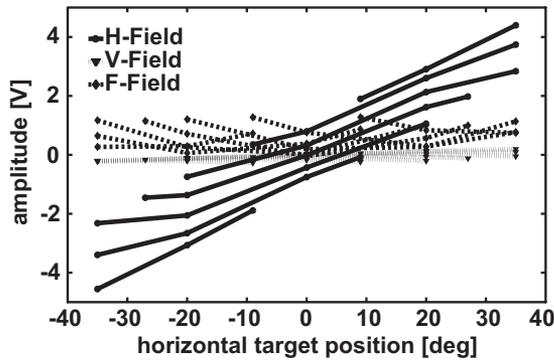
FIG. 6. Raw ring signals for the horizontal (H-field, solid lines, black dots), vertical (V-field, dotted lines, black triangles), and frontal (F-field, dashed lines, black diamonds) fields as function of horizontal gaze position for head orientations $R = \{\pm35, \pm20, \pm9, 0\}$ deg and $\phi = \{0, 180\}$ deg. Subject PB.

A direct comparison of the calibrated endpoints for the DMI method and the SSC technique can be seen in Fig. 9*A*. Open circles denote DMI endpoints and gray circles SSC endpoints. The intersections of the light gray rings and spokes correspond to the targets on the LED sky. Note that the multiple endpoints at one LED location result from different gaze shifts to the same spatial location, not from repetitions of the same head–eye combination. The mean difference between the SSC and DMI endpoints for both the horizontal and the vertical components is 0.00 deg and the SD is 0.68 deg for the horizontal component and 0.67 deg for the vertical component. Thus despite the pronounced differences for the raw eye target endpoints of the DMI and SSC signals, as depicted in Fig. 7, the network is able to calibrate the data.

SACCADES DURING THE TEST PARADIGM. After training, the networks were tested on an independent data set obtained during the test paradigm, in which the subject made head-unrestrained gaze shifts toward peripheral targets. Figure 9*B* shows spatial trajectories for subject PB to the most eccentric circle of the LED sky ($R = 35$ deg). Red lines indicate DMI data, blue lines SSC gaze data, and black dashed lines the head-movement trajectories. Gray symbols denote target positions, whereas the white central symbol is the fixation LED. Note that the ring and the SSC are worn on different eyes. Thus it is expected that the
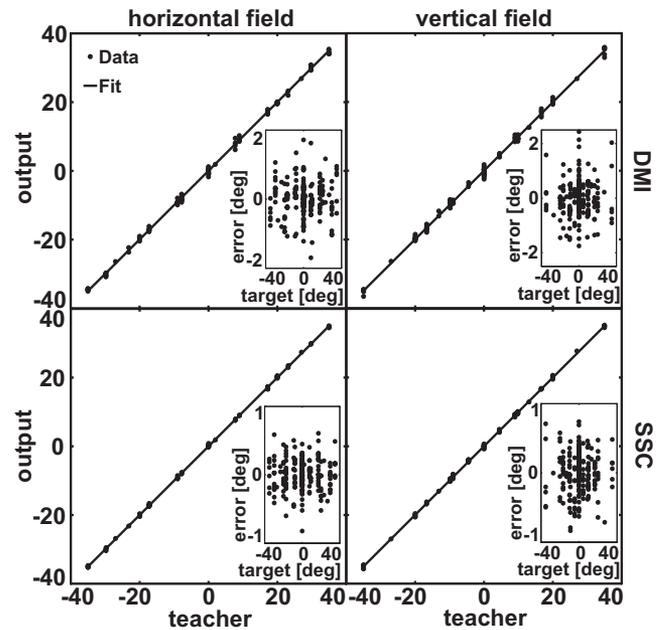
FIG. 8. Linear regressions of the calibrated neuronal network output and the teacher values for the horizontal (*left column*) and vertical (*right column*) component of the DMI method (*top row*) and the SSC technique (*bottom row*) for subject PB. *Insets* in each panel depict the corresponding errors, i.e., teacher value minus network output value.

eye-movement trajectories will be similar, but not necessarily identical. Indeed, small differences may be observed in the gaze trajectories of Fig. 9*B*. It is important to note that these differences were not systematic and were not reproduced between trials. For example, toward the end of the rightward horizontal gaze shift the DMI and SSC signals seem to diverge. This feature was not due to a calibration artifact, of either recording method, because it did not occur on other trials. Rather, it might be due to small differences in binocular gaze control and differences in the amplitude of blinks by the left and right eyes.

Figure 10 depicts in an analogous manner the temporal traces for subject JG. All 72 trials of the head-unrestrained test paradigm are shown as one continuous trace for both the
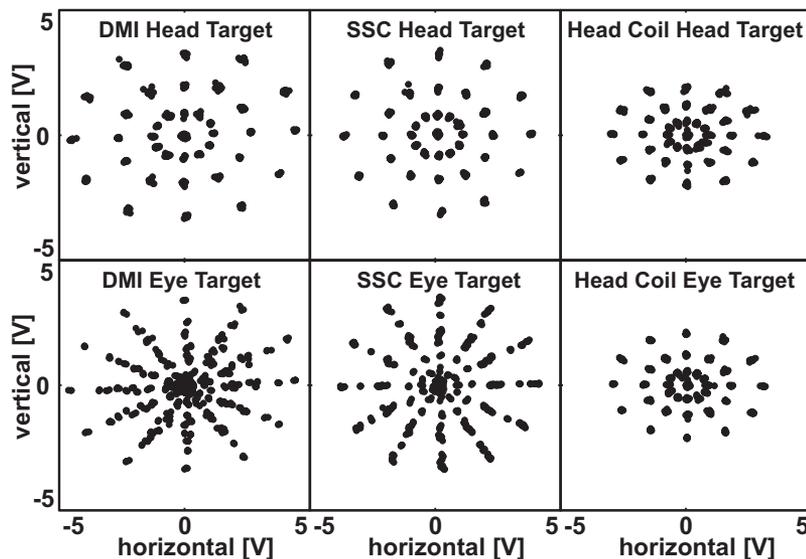
FIG. 7. Raw endpoints for the DMI method (*left column*), the SSC technique (*middle column*), and the head coil (*right column*) for subject PB. *Top row*: endpoints extracted during presentation of the head target. *Bottom row*: endpoints extracted during presentation of the eye target.

TABLE 3. *Coefficients of the fits between the neuronal network output and the teacher value for horizontal and vertical components of the DMI method and the SSC technique for subject PB*

95% Confidence Intervals					
Slope	Intercept	Adj. r^2	RMSE	N	Technique/Component
0.999 (0.995 1.003)	−0.006 (−0.068 0.056)	0.99	0.46	109	DMI horizontal
0.998 (0.992 1.005)	0.017 (−0.062 0.097)	0.99	0.59	109	DMI vertical
0.999 (0.998 1.002)	−0.002 (−0.031 0.028)	0.99	0.22	109	SSC horizontal
0.999 (0.996 1.002)	−0.007 (−0.047 0.034)	0.99	0.30	109	SSC vertical

horizontal and vertical gaze components. The *insets* highlight instants with the largest differences between SSC and DMI signals. We found no systematic relation between these differences and target location. The mean difference for the horizontal component is 0.30 deg (SD 0.64 deg) and 0.34 deg (SD 0.72 deg) for the vertical component.

Temporal gaze component, velocity, and acceleration plots of subject RW to four selected targets are shown in Fig. 11. The DMI signals are plotted as red lines, the SSC signals as blue lines. Different hues denote the different trials. The traces have been temporally aligned such that the gaze saccade onsets coincide. Note that the DMI and SSC signals of the individual trials are in good agreement, even for the acceleration profiles. Again, because ring and SSC were worn on different eyes small differences in the traces are most likely due to differences in binocular oculomotor control and not due to the calibration of either signal. The head-free DMI method could thus be used for detailed trajectory and gaze kinematics analysis as has been done in head-restrained paradigms (e.g., Van Opstal and Van Gisbergen 1987).

In Fig. 12 the gaze and reconstructed eye-in-head traces of the DMI method (red lines) and the SSC technique (blue lines) for two target locations (gray lines) are shown. The head trace is depicted as a black dashed line (data from subject PB). The signals from both methods are very similar. Note the small correcting saccade in the gaze and eye-in-head traces toward the vertical 20 deg target for both the DMI and the SSC signals. Note also that the head traces reach the target because the

subject has visual feedback by the laser pointer. These large head movements elicit counterrotation of the eyes, such that the eyes keep fixating the target while the head is still moving. The operation of the vestibular ocular reflex can thus be seen in both signals.

DISCUSSION

We have shown that the extended DMI method is a valuable tool for measuring head-unrestrained 2D gaze shifts. The simultaneous recordings of the SSC technique and the extended DMI method are in good agreement. Although in our current setup the resolution of 0.3 deg obtained with the extended DMI method is somewhat inferior to that of the SSC technique (0.2 deg) it remains well within the resolution of the oculomotor system. We believe that the signal-to-noise ratio can still be improved substantially. Most of the noise in the DMI method is due to electronic limitations imposed by the Remmel system (see following text).

Although we regarded the SSC signal as the perfect gold standard for comparison with the DMI method, this assumption need not be valid at all times. For example, coil slippage and minor pulling forces induced by the lead wires could have an influence on the trajectories and kinematics of saccades, or lead to an increase of blinking activity, and could thus be partly responsible for small trial-to-trial differences between the DMI and SSC signals, as in Figs. 9*B* and 10. On the other hand, because we recorded movements from both eyes simultaneously, small differences in binocular control signals, most notably due to differences in oculomotor plant characteristics (e.g., medial rectus vs. lateral rectus eye muscles), also likely contribute to these differences.

Stability of the DMI system

The extended DMI method as presented here with the DMI assembly mounted on a plastic glasses frame is a low-cost solution that is easy to implement. The frame's position remains stable relative to the ring and no disturbances of the signal were observed during highly accelerated gaze shifts. However, special care should be taken to ensure that the pickup coil and the anticoil are fixed in the same plane (not necessarily close to each other if the magnetic fields are reasonably homogeneous) to ensure a minimal head-orientation–dependent residue of the three primary field components. Furthermore, depending on the exact size of the glasses frame the field of view can be somewhat limited. In our case some subjects reported to have difficulties seeing the far upward $(R, \phi) = (35, 90)$ deg target. Moreover, in its current form, subjects with corrected-to-normal vision will not be able to wear their own
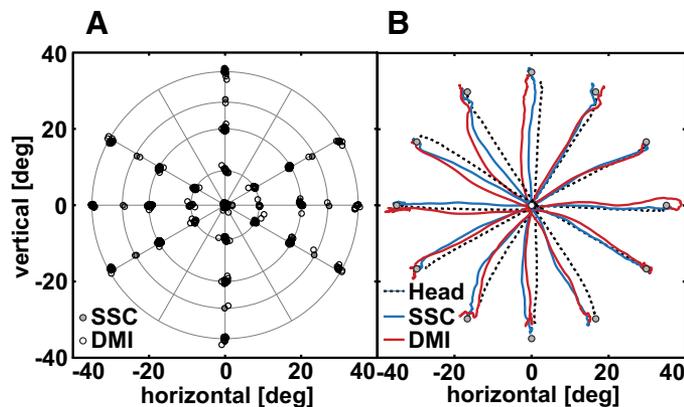
FIG. 9. *A*: calibrated fixation points for both the DMI method (open circles) and the SSC technique (gray circles) for subject PB. Light gray rings and spokes denote the LED sky. On each intersection of the rings and spokes a stimulus LED is installed. *B*: calibrated spatial traces for the DMI method (red lines), the SSC technique (blue lines), and the head (dashed line) for subject PB. Fixation point is indicated by the white circle and target positions by gray circles. Note small differences between SSC and DMI gaze trajectories. Note also that the SSC and the DMI ring were worn on different eyes.
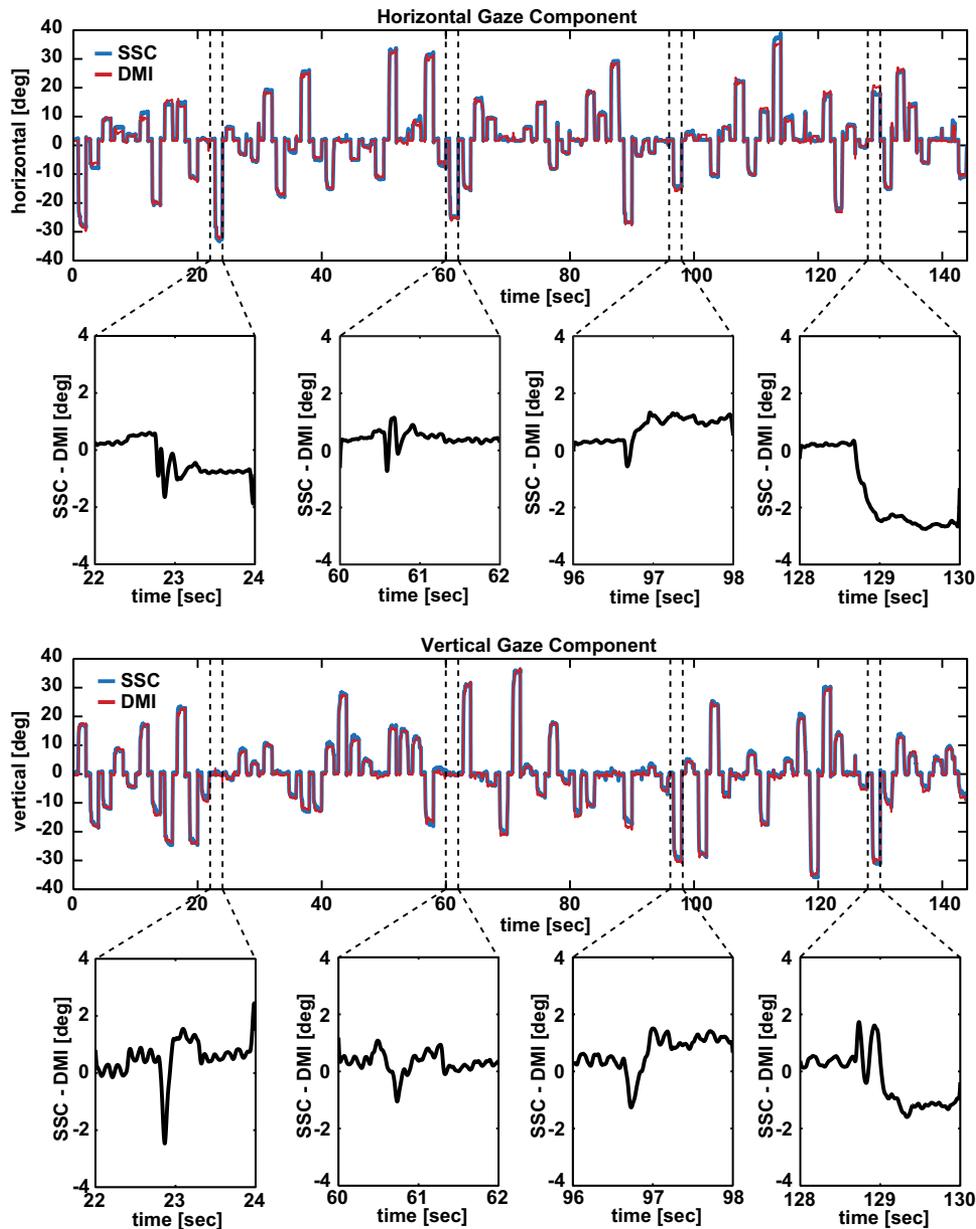
FIG. 10. Calibrated temporal traces of the test paradigm for the DMI method (red lines) and the SSC technique (thick blue lines) for subject JG. *Top*: horizontal gaze component. *Bottom*: vertical gaze component. Some of the largest differences between the 2 methods are highlighted in the subplots for 4 trials. Differences were not systematic and typically small (<1 deg).

glasses. However, the glasses frame could be easily modified so that exchangeable lenses could be attached.

The glasses frame turned out to be a far better solution than a bite board. Pilot measurements with a bite board yielded substantial vibration artifacts, especially in the vertical channel that severely disturbed the measurements. In addition to this technical issue the glasses frame is much better suited for the use in patients for whom a bite board is considered a serious burden in addition to the invasive nature of techniques based on electromagnetism.

We also tested the intersession stability of the assembly, by applying the V_{net} calibration of a given session to the data obtained on a different recording day. However, the differences, which on average was >2 deg, were found to be too large (data not shown). Probably, day-to-day variations in the play dough used to roughly center the assembly in front of the ring may have caused these differences. As a result, it was deemed necessary to calibrate the system before each use.

Measurement range and calibration

Note that the extended DMI method is not limited to the 2D range of ±35 deg tested here. Provided the calibration subset is chosen appropriately the range can be readily extended to the full 360 deg. For the range tested here, a calibration data set of 109 unique eye–head combinations already sufficed to obtain a good calibration. It is important to choose the set of unique eye–head combinations in such a way that most points fall into the nonlinear and nonmonotonic part of the ring's signal. These are usually the most extreme eye positions. In this context it is also interesting to note that the used networks (four input units, four hidden units, one output) could theoretically use 40 (20 weights and 20 biases) parameters. In practice, however, the number of effective parameters used was typically between 20 and 25. This order of magnitude seems surprisingly small when compared with the calibration routine for the *head-restrained* DMI method described by Bour et al. (1984) that needed 36
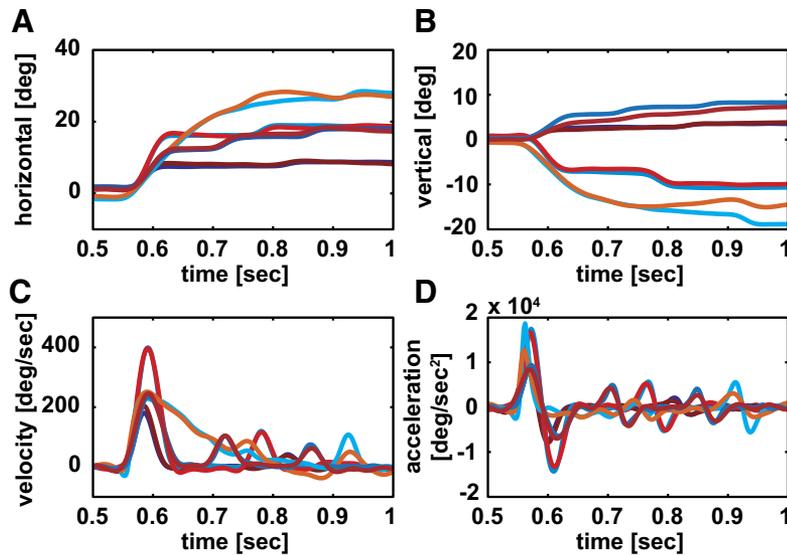
FIG. 11. Temporal, velocity, and acceleration plots for the DMI method (red lines) and the SSC technique (blue lines) of 4 trials (different line hues) from subject RW. Traces are plotted from stimulus onset to stimulus offset and are temporally shifted so that saccade onsets are aligned. *A*: horizontal gaze components. *B*: vertical gaze components. *C*: velocity profiles. *D*: acceleration profiles.

parameters to correct for the direction-dependent signal non-linearity. Note that Bos et al. (1988) described an analytical method to reduce the number of parameters to only six; their calibration routine was based on the theoretical assumption that the axes of ring and pickup coil would exactly align, a requirement that is hard to realize in practice. In the *head-unrestrained* setting the nonmonotonic ring signal with its pickup coil–induced asymmetry and the complex primary field remnants can be calibrated with roughly the same number of parameters using the calibration routine presented here. More important, by using a simple model-free feedforward neuronal network, no special care needs to be taken to account for the complex V_{net} signal. In addition, there is no need for the use of micromanipulators to exactly center the pickup coil in front of the ring (Malpeli 1998). As long as the pickup coil and ring are roughly aligned the network will be able to disambiguate the nonmonotonic ring signal.

As we have shown in our previous study (Bremen et al. 2007) the extended DMI method can in principle be used to record over the entire 360 deg range. Due to limitations in the target arrays in our current setup the recording range was restricted to 35 deg in all directions. As a consequence of how the complex (and unknown) geometry of the assembly enters the equations for the DMI method (*Eq. 1*) it is not possible to simply extrapolate recorded signals beyond the range for which

the system is actually calibrated. Thus when measuring gaze shifts over a larger range a calibration procedure is required that covers this extended range. Although the resolution within the 35 deg range remained fairly constant, and although the application of three orthogonal magnetic fields theoretically allows for a constant resolution within the entire hemifield, the behavior of the DMI method for a larger measurement range will have to be established by future experiments.

Recording hardware

It is noteworthy that the head-unrestrained DMI method is not restricted to use with the Remmel recording hardware. As long as three perpendicular primary magnetic fields are provided any recording hardware can be used. For example, the lock-in amplifiers of Princeton Applied Research (model PAR 128A) have been used successfully in the head-restrained DMI method (Bour et al. 1984; Chaturverdi and Van Gisbergen 2004; Ottes et al. 1984; Van Opstal and Van Gisbergen 1987) and could also be applied with head-free DMI, as long as the input sensitivity is adapted to the signal strength of V_{net} plus ring. Note that when using the Remmel eye monitor system it is important to use low-impedance primary field coils because this will drastically increase the S/N ratio of the ring signal. The use of aluminum bars for field generation could also have a beneficial effect on the S/N ratio and thus on the system's resolution.

Comparison with video techniques

When comparing the extended DMI method to currently available video eye tracking systems basically the same points that hold true for the SSC technique can be noted as well. The invasive nature of the DMI method can be considered a disadvantage, especially when working with patients or children. However, with DMI head-unrestrained measurements are possible; moreover, measurements can be performed in total darkness, even with closed eyelids, and at arbitrarily high sampling rates. The glasses frame holding the DMI assembly is lightweight in comparison with video helmets so that the glasses frame will not disturb the head-movement kinematics.
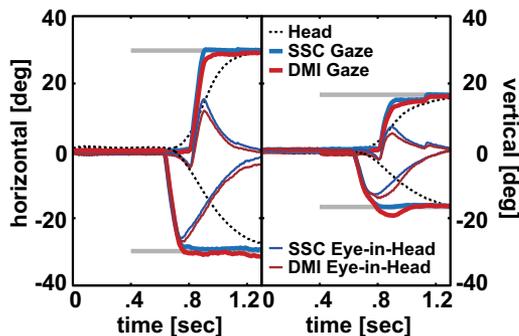
FIG. 12. Calibrated temporal gaze and eye-in-head traces of the DMI method (red lines) and the SSC technique (blue lines) for subject PB. Head signal is denoted with a dashed line. Light gray horizontal bars indicate target positions ($R = [35, 30]$, $\Phi = [35, 210]$). *Left*: horizontal component. *Right*: vertical component.

When comparing the costs of the DMI, SSC, and video systems, current video-based techniques are by far the most expensive. However, even the SSCs cost well over US$100, per coil, so that with an average lifetime of four to six experiments an SSC experiment will typically cost about US$25. These running expenses do not apply to the DMI method (a single gold-plated copper ring suffices), which renders it an accurate, efficient, simple, and relatively low cost recording technique.

Binocular recordings

With minor modifications of the current assembly, simultaneous recordings of both eyes are also possible, thus allowing the study of head-free vergence eye movements (for head-fixed binocular DMI see, e.g., Chaturvedi and van Gisbergen 2000). However, torsional eye movements (Hess et al. 1992; Houben et al. 2006) cannot be measured with the DMI method.

Experimental animals

Especially in experimental animals the head-unrestrained DMI method will be a promising alternative to the SSC technique. Implantation of the ring is less invasive than that of the SSC because one need not guide the lead wire subcutaneously to a connector on top of the animal's head (Bour et al. 1984; Judge et al. 1979). Instead, the ring is implanted by simply opening and closing of the conjunctiva, which heals within a few days. More important, however, the absence of a lead wire renders the DMI method less vulnerable to malfunction than the SSC technique. In comparison to its use in human subjects, as described herein, the DMI method can be applied even more robustly in laboratory animals because the DMI assembly can be rigidly fixed to the animal's skull. This will ensure that the day-to-day geometry of the DMI assembly and ring is fixed for laboratory animals, and that therefore calibration of the ring signal will progressively improve as more data accumulates with every new recording day. Once a good calibration network has been determined it can be applied to the data recorded on different days, without the need for extensive calibration sessions.

However, because it is time consuming, and often impossible, to train animals to perform the type of coordinated eye–head movements as applied in the present study, a different calibration approach may have to be used. Note that in principle two signals are needed for the calibration: *1*) the head-in-space signal (head coil) and *2*) the eye-in-head signal (DMI ring). The head coil can easily be calibrated beforehand, for example, by determining the gains of the coil as it is rotated without the subject in the experimental chamber. This is a standard calibration routine used for example when implanting eye coils in cats or monkeys. Then, the animal can be trained in a standard paradigm to make head-free gaze shifts to peripheral visual targets. The information of the calibrated head position can then be related to the measured (and known) eye orientation in space from which the eye-in-head orientation

can readily be reconstructed. In this way a catalog of eye orientations for a given head orientation is collected. After a number of sessions sufficient data could be collected to calibrate the ring's signal. It is, however, to be expected that the collection of such a catalog will take longer than the procedure described here for human subjects.

REFERENCES

Allik J, Rauk M, Luuk A. Control and sense of eye movement behind closed eyelids. *Perception* 10: 39–51, 1981.

Bos JE, Reulen JPH, Boersma HJ, Ditters BJ. Theory of double magnetic induction (DMI) for measuring eye movements: correction for nonlinearity and simple calibration in two dimensions. *IEEE Trans Biomed Eng* 35: 733–739, 1988.

Bour LJ, Van Gisbergen JAM, Bruijns J, Ottes FP. The double magnetic induction method for measuring eye movement—results in monkey and man. *IEEE Trans Biomed Eng* 31: 419–427, 1984.

Bremen P, Van der Willigen RF, Van Opstal AJ. Using double-magnetic induction to measure head-unrestrained gaze shifts. I. Theory and validation. *J Neurosci Methods* 160: 75–84, 2007.

Chaturvedi V, Van Gisbergen JA. Stimulation in the rostral pole of monkey superior colliculus: effects on vergence eye movements. *Exp Brain Res* 132: 72–78, 2000.

Collewijn H, Van der Mark F, Jansen TC. Precise recording of human eye movements. *Vision Res* 15: 447–450, 1975.

Hess BJ, Van Opstal AJ, Straumann D, Hepp K. Calibration of three-dimensional eye position using search coil signals in the rhesus monkey. *Vision Res* 32: 1647–1654, 1992.

Hofman P, Van Opstal AJ. Spectro-temporal factors in two-dimensional human sound localization. *J Acoust Soc Am* 103: 2634–2648, 1998.

Houben MMJ, Goumans J, Van der Steen J. Recording three-dimensional eye movements: scleral search coils versus video oculography. *Invest Ophthalmol Vis Sci* 47: 179–187, 2006.

Judge SJ, Richmond BJ, Chu FC. Implantation of magnetic search coils for measurement of eye position: an improved method. *Vision Res* 20: 535–538, 1979.

MacKay DJC. Bayesian interpolation. *Neural Comput* 4: 415–447, 1992.

Malpeli JG. Measuring eye position with the double magnetic induction method. *J Neurosci Methods* 86: 55–61, 1998.

Ottes FP, Van Gisbergen JAM, Eggermont JJ. Metrics of saccade responses to visual double stimuli: two different modes. *Vision Res* 24: 1169–1179, 1984.

Remmel RS. An inexpensive eye movement monitor using the scleral search coil technique. *IEEE Trans Biomed Eng* 31: 388–390, 1984.

Reulen JP, Bakker L. The measurement of eye movement using double magnetic induction. *IEEE Trans Biomed Eng* 29: 740–744, 1982.

Robinson DA. A method of measuring eye movement using a scleral search coil in a magnetic field. *IEEE Trans Biomed Eng* 10: 137–145, 1963.

Van Opstal AJ, Van Gisbergen JAM. Skewness of saccadic velocity profiles: a unifying parameter for normal and slow saccades. *Vision Res* 27: 731–745, 1987.